THE PHOTOGRAMMETRIC RECORD

The Photogrammetric Record (2013)
DOI: 10.1111/phor.12010

COMBINED BUNDLE BLOCK ADJUSTMENT WITH SPACEBORNE LINEAR ARRAY AND AIRBORNE FRAME ARRAY IMAGERY

YONGJUN ZHANG (zhangyj@whu.edu.cn)
LIWEN LIN[1] (lin.1128@buckeyemail.osu.edu)
MAOTENG ZHENG (tengve@163.com)
JINXIN XIONG (einbetter1995@hotmail.com)
Wuhan University, Wuhan, China

[1]*Also at Ohio State University, Columbus, USA*

Abstract

The integration of multi-source earth observation data has become one of the most important developments in photogrammetry. A combined adjustment with linear array and frame array imagery (CALFI) is established in this paper. The mathematical model of CALFI is based on the conventional single-source bundle adjustment. A revised recursive partitioning technique is utilised to solve the large normal matrix of CALFI; the orientation parameters of the linear array imagery are arranged at the border of the reduced normal matrix to save both memory and computation time. The experimental results on simulated data show that both the accuracy and the condition index of the CALFI model are superior to the conventional bundle adjustment model with either linear array or frame array imagery separately due to the higher redundancy.

KEYWORDS: combined bundle adjustment, condition index, frame array imagery, linear array imagery, multi-source data processing, normal matrix

INTRODUCTION

ALONGSIDE THE RAPID DEVELOPMENTS and widespread applications of a new generation of remote sensing sensors (digital frame cameras and line scan cameras, in addition to the use of differential global navigation satellite systems (GNSS) and inertial measurement units (IMUs)), the integration of different types of sensor information and the fusion of multi-source datasets have become challenging topics in photogrammetry (Ackermann, 1995; Zhang et al., 2005; 2011). Bundle block adjustment, which is one of the most important processes in photogrammetry, also has an impact on the integration of multi-sensor datasets. A combination of multiple sensors that employ different physical sensor models can provide complementary and redundant information for aerial triangulation (Schenk, 2003). This strategy can provide more comprehensive observations of the object of interest and improve the quality of bundle block adjustment. The observations of

differential GNSS/IMU, also called the positioning and orientation system (POS), have been successfully introduced into block adjustments (Greening et al., 2000). The integration of these observations into the adjustment greatly decreases the required number of ground control points (GCPs) required and contributes to a higher level of automation of the bundle adjustment (Wolf, 1983).

Frame array images (sometimes termed matrix array images) and linear array images are the two main sources of imagery in photogrammetry. Both types have their advantages and disadvantages. Frame array imagery has a stable geometric configuration, and the corresponding photogrammetric processing technologies are also very mature. However, it is difficult to manufacture large format frame cameras that can be applied in satellite photogrammetry. A frame camera is therefore usually limited to aerial photogrammetry. Compared with a frame camera, a linear array sensor is more flexible in terms of camera design and is comparatively easier to manufacture (Gruen and Zhang, 2003; Wang et al., 2004). Linear scanners have been widely applied in both aerial and satellite photogrammetry; however, due to the special imaging principle, the geometric configuration of linear array imagery is not always stable (Lee et al., 2000). The photogrammetric processing of linear array imagery is therefore more complicated than frame array imagery (Cariou and Chehdi, 2008).

The above description of the characteristics of the two types of imagery suggests that they are mutually complementary to each other and therefore have great potential for integration. Wang et al. (2004) proposed a linear-matrix CCD array (LMCCD) camera for satellite photogrammetry, which integrates three linear array scanners with four small frame CCD arrays located on each side of the two ends of the nadir linear array. The simulated experiment of bundle adjustment shows that the combination of the two types of images obtained from LMCCD makes considerable contributions in aerial triangulation; but LMCCD requires a specific camera with both linear array and frame array CCDs mounted on the same platform, which is very difficult to manufacture. A combined aerial triangulation with frame cameras, panoramic sensors and three linear scanners was developed by Habib and Beshah (1998). The simulated studies showed promising accuracy by the fusion of imagery with different imaging modes in multi-sensor aerial triangulation. Li et al. (2008) integrated spaceborne linear array images with aerial frame array images to achieve higher geopositioning accuracy in shoreline mapping. Straight lines and planar patches were used as primitives by Shin et al. (2007) for the triangulation of optical imagery and lidar data. In general, however, most of the research related to the integration of linear array and frame array images mainly addressed the adjustment precision. The integration of two types of imagery from different sensor platforms on different flight missions can, in fact, make a considerable contribution to the geometric configuration of combined adjustment, which can greatly assist in obtaining robust and reliable estimations of unknowns.

This paper proposes the concept and methods of combined block adjustment with multi-source linear array and frame array imagery (CALFI) in order to draw more attention to the promising potential of integrating such multi-source imagery. The next section briefly describes CALFI and its features, including the proposed mathematical model of the method. In addition, a detailed approach for solving the large number of normal equations generated is discussed. Subsequently, the experiments conducted for three different modes with simulated datasets are presented and analysed, and conclusions are drawn.

General Concept of the Combined Block Adjustment

CALFI is a process which provides an integrated bundle block adjustment with multi-senor linear array and frame array imagery of the same ground area with the aid of

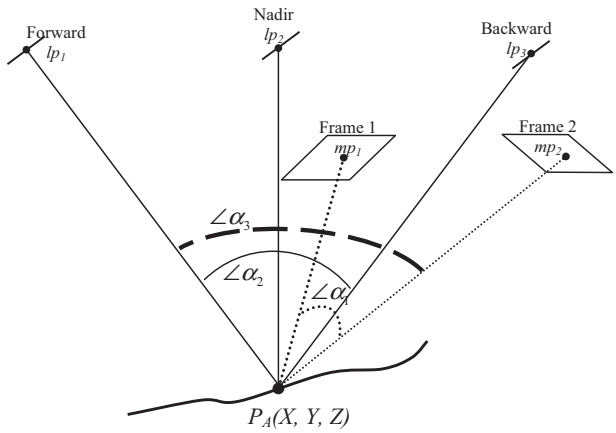

FIG. 1. Joint observations with multi-source linear array and frame array images.

POS observations and a few GCPs. All unknowns, including the exterior orientation (EO) parameters, the object space coordinates of tie points and additional parameters, can be simultaneously estimated using this strategy. In CALFI, linear array or frame array data can be observed by airborne or spaceborne sensors; for example, frame array imagery can be obtained by airborne cameras and linear array imagery can be obtained either by airborne or spaceborne linear scanners. By integrating multi-source linear array and frame array imagery with multiple flying heights, different viewing angles and various imaging principles, CALFI is expected to obtain more comprehensive bundle adjustment results than that provided by frame array or linear array images alone.

As illustrated in Fig. 1, a certain area is jointly observed by three linear array cameras (pointing forward, backward and vertically downwards) and a frame array camera. Assuming that a ground point P_A is photographed on forward (lp_1), nadir (lp_2) and backward (lp_3) views of the linear array cameras, as well as on frame image 1 (mp_1) and frame image 2 (mp_2) of a frame array camera, the ground point P_A now constitutes the necessary observing conditions for joint processing of linear array and frame array images. Theoretically, CALFI has the advantages outlined in the three paragraphs below.

Greater Redundancy

Since any given ground point is being imaged by two types of cameras in CALFI, it has more corresponding image points than with either a block adjustment with linear array imagery (BALI) or with a block adjustment with frame array imagery (BAFI) separately, because both of these merely employ a single type of imagery. The combined strategy of CALFI takes advantage of more observations and a greater number of redundancies to improve the robustness of the bundle adjustment.

Possible Increase in the Convergence Angle

When a ground point is simultaneously photographed on linear array and frame array images, and there is no inclusive relationship between the linear array and frame array bundles, the maximum convergence angle of the rays to the ground point would be increased due to the combination of the two types of imagery. As shown in Fig. 1,

the maximum convergence angle of point P_A will be $\angle\alpha_1$ or $\angle\alpha_2$ if only frame array images or linear array images, respectively, are used, while the maximum convergence angle will be $\angle\alpha_3$ if both frame array and linear array images are used. Increasing the convergence angle contributes significantly to an improvement in the vertical accuracy of the block adjustment.

Better Observational Structure

When a linear scanner and a frame camera are carried on different platforms with different trajectories, the observational geometry will be more solid and comprehensive, which also means a better observational structure in the adjustment system due to the photography with different orbital/flying heights, different angles of view and different imaging modes.

MATHEMATICAL MODEL OF THE COMBINED BLOCK ADJUSTMENT

Essentially, CALFI is a combined bundle adjustment model that integrates two different types of imagery that possess different geometric structures. Therefore, the mathematical model is constructed by combining the conventional models BALI and BAFI.

Observation Equation of Frame Array Imagery

The geometry of frame array imagery is based on the perspective projection. The projection centre P, a ground point $P_A(X,Y,Z)$ and its corresponding image point (x,y) satisfy the collinearity equation. Assuming there are n frame array images and m image points, then the observation equation of the jth image point on the ith image is

$$\underset{2\times1}{\mathbf{v}_{ij}} = \underset{2\times6}{\mathbf{A}_{ij}}\,\underset{6\times1}{\mathbf{tm}_i} + \underset{2\times3}{\mathbf{B}_{ij}}\,\underset{3\times1}{\mathbf{X}_j} - \underset{2\times1}{\mathbf{l}_{ij}} \quad (i = 1,\ldots,n,\ j = 1,\ldots,m) \text{ with weight } \mathbf{P}_m \tag{1}$$

where: $\underset{6\times1}{\mathbf{tm}_i} = (\mathrm{d}X_{si}, \mathrm{d}Y_{si}, \mathrm{d}Z_{si}, \mathrm{d}\phi_i, \mathrm{d}\omega_i, \mathrm{d}\kappa_i)^{\mathrm{T}}$ is the vector of EO parameters of the ith image; $\underset{3\times1}{\mathbf{X}_j} = (\mathrm{d}X_j, \mathrm{d}Y_j, \mathrm{d}Z_j)^{\mathrm{T}}$ is the vector of the object space coordinate of the jth image point; $\underset{2\times6}{\mathbf{A}_{ij}} = \begin{bmatrix} a_{11}^{ij} & a_{12}^{ij} & a_{13}^{ij} & a_{14}^{ij} & a_{15}^{ij} & a_{16}^{ij} \\ a_{21}^{ij} & a_{22}^{ij} & a_{23}^{ij} & a_{24}^{ij} & a_{25}^{ij} & a_{26}^{ij} \end{bmatrix}$ and $\underset{2\times3}{\mathbf{B}_{ij}} = \begin{bmatrix} -a_{11}^{ij} & -a_{12}^{ij} & -a_{13}^{ij} \\ -a_{21}^{ij} & -a_{22}^{ij} & -a_{23}^{ij} \end{bmatrix}$ are the design matrices composed of partial derivatives of the collinearity equation with respect to the EO parameters and object space coordinates; and $\underset{2\times1}{\mathbf{v}_{ij}} = [\,vx_{ij} \quad vy_{ij}\,]^{\mathrm{T}}$ and $\underset{2\times1}{\mathbf{l}_{ij}} = [\,lx_{ij} \quad ly_{ij}\,]^{\mathrm{T}}$ are the residual and discrepancy vectors of observations, respectively.

Observation Equation of Linear Array Imagery

It is impossible in practice to calculate the EO parameters of every scanning line of linear array imagery; thus, a suitable sensor orientation model is needed for georeferencing such imagery. At present, there are mainly two approaches for the orientation of linear array imagery (Poli, 2004): (1) a rigorous sensor model, such as a piecewise polynomial model and an orientation image model; and (2) an empirical model, such as a rational function model, a direct linear transformation, an affine transformation, and so on. Because of the sta-

ble and smooth trajectory of the three spaceborne linear array sensors (each with a different viewing angle) within a short distance, a quadratic polynomial (Gruen and Zhang, 2003; Li et al., 2009) is employed to model the trajectory of a linear array image sensor in this paper. Therefore, the EO parameters of a linear array image can be expressed by quadratic polynomials (Gugan, 1987; Orun and Natarajan, 1994; Gruen and Zhang, 2003; Kocaman and Gruen, 2008) as follows:

$$\begin{cases} X_s^t = X_{s0} + \dot{X}_s t + \ddot{X}_s t^2 \\ Y_s^t = Y_{s0} + \dot{Y}_s t + \ddot{Y}_s t^2 \\ Z_s^t = Z_{s0} + \dot{Z}_s t + \ddot{Z}_s t^2 \\ \phi^t = \phi_0 + \dot{\phi}\, t + \ddot{\phi}\, t^2 \\ \omega^t = \omega_0 + \dot{\omega}\, t + \ddot{\omega}\, t^2 \\ \kappa^t = \kappa_0 + \dot{\kappa}\, t + \ddot{\kappa}\, t^2 \end{cases} \tag{2}$$

where $[X_s^t, Y_s^t, Z_s^t, \phi^t, \omega^t, \kappa^t]^{\mathrm{T}}$ represent the EO parameters of the tth scanning line; $[X_{s0}, Y_{s0}, Z_{s0}, \phi_0, \omega_0, \kappa_0]^{\mathrm{T}}$ are the EO parameters of the first scanning line; and $[\dot{X}_s, \dot{Y}_s, \dot{Z}_s, \dot{\phi}, \dot{\omega}, \dot{\kappa}]^{\mathrm{T}}$ and $[\ddot{X}_s, \ddot{Y}_s, \ddot{Z}_s, \ddot{\phi}, \ddot{\omega}, \ddot{\kappa}]^{\mathrm{T}}$ are the linear and quadratic coefficients of the EO parameters, respectively.

The geometry of linear array imagery is also a linear perspective projection, in which the collinearity condition is still satisfied. Assuming the whole surveying area includes n trajectories and m linear array image points, the observation equation of the jth image point in the ith trajectory can be described as

$$\mathbf{v}_{ij} = \underset{2\times 18}{\mathbf{A}_{ij}}\ \underset{18\times 1}{\mathbf{tl}_i} + \underset{2\times 3}{\mathbf{B}_{ij}}\ \underset{3\times 1}{\mathbf{X}_j} - \mathbf{l}_{ij} \quad (i = 1, \ldots, n,\ j = 1, \ldots, m) \text{ with weight } \mathbf{P}_i \tag{3}$$

where: $\underset{18\times 1}{\mathbf{tl}_i}$ is the vector of the quadratic polynomial coefficients in the ith trajectory, namely, $\underset{18\times 1}{\mathbf{tl}_i} = \left[\mathrm{d}X_{s0}^i, \mathrm{d}Y_{s0}^i, \mathrm{d}Z_{s0}^i, \mathrm{d}\phi_0^i, \mathrm{d}\omega_0^i, \mathrm{d}\kappa_0^i, \mathrm{d}\dot{X}_s^i, \mathrm{d}\dot{Y}_s^i, \mathrm{d}\dot{Z}_s^i, \mathrm{d}\dot{\phi}^i, \mathrm{d}\dot{\omega}^i, \mathrm{d}\dot{\kappa}^i, \mathrm{d}\ddot{X}_s^i, \mathrm{d}\ddot{Y}_s^i, \mathrm{d}\ddot{Z}_s^i, \mathrm{d}\ddot{\phi}^i, \mathrm{d}\ddot{\omega}^i, \mathrm{d}\ddot{\kappa}^i\right]^{\mathrm{T}}$; and $\underset{2\times 18}{\mathbf{A}_{ij}} = \left[\underset{2\times 6}{\mathbf{C}} \quad t\underset{2\times 6}{\mathbf{C}} \quad t^2\underset{2\times 6}{\mathbf{C}}\right]$ is the design matrix with respect to $\underset{18\times 1}{\mathbf{tl}_i}$, in which the sub-matrix $\underset{2\times 6}{\mathbf{C}}$ is the partial derivatives of the EO parameters of the collinearity equation.

Observation Equation of POS Data of Frame Array Imagery

The observation equations of the POS data with regard to frame array imagery are well known in the literature and usually have the following general form:

$$\underset{6\times 1}{\mathbf{v}_{mpos}} = \underset{6\times 6}{\mathbf{A}_{mpos}}\ \underset{6\times 1}{\mathbf{tm}_i} - \underset{6\times 1}{\mathbf{l}_{mpos}} \quad \text{with weight } \mathbf{P}_{mpos} \tag{4}$$

where $\underset{6\times 6}{\mathbf{A}_{mpos}} = \underset{6\times 6}{\mathbf{E}}$ is the design matrix of POS observations where $\underset{6\times 6}{\mathbf{E}}$ is a 6×6 identity matrix; $\underset{6\times 1}{\mathbf{tm}_i}$ is the vector of the EO parameters of the ith image; and $\underset{6\times 1}{\mathbf{v}_{mpos}}$ and $\underset{6\times 1}{\mathbf{l}_{mpos}}$ are respectively the residual and discrepancy vectors of the POS observations. If the systematic

errors in the POS observations are to be considered, the corresponding unknowns and coefficients should be added to the above equation.

Observation Equation of POS Data of Linear Array Imagery

The observation equation of the POS data of linear array imagery should be built in terms of the quadratic polynomial function, which is used as the orientation model of linear array imagery in this paper. Assuming there are n POS measurements, then the observation equation of the tth scanning line is

$$\underset{6\times1}{\mathbf{v}_{lpos}} = \underset{6\times18}{\mathbf{A}_{lpos}}\ \underset{18\times1}{\mathbf{tl}_i} - \underset{6\times1}{\mathbf{l}_{lpos}} \quad \text{with weight } \mathbf{P}_{lpos} \tag{5}$$

where $\underset{6\times18}{\mathbf{A}_{lpos}} = \left[\underset{6\times6}{\mathbf{E}} \quad t\underset{6\times6}{\mathbf{E}} \quad t^2\underset{6\times6}{\mathbf{E}}\right]$ is the design matrix of POS observation with, once again, $\underset{6\times6}{\mathbf{E}}$ being a 6×6 identity matrix; $\underset{18\times1}{\mathbf{tl}_i}$ is the vector of the quadratic polynomial coefficients of the ith trajectory; and $\underset{6\times1}{\mathbf{v}_{lpos}}$ and $\underset{6\times1}{\mathbf{l}_{lpos}}$ are the residual and discrepancy vectors of the POS observations, respectively. Again, if the systematic errors of the POS observations are to be considered, the corresponding unknowns and coefficients should be added.

Observation Equations of CALFI

Incorporating the observation equations from equation (1) to equation (5), the following mathematical model for CALFI can be derived:

$$\begin{cases} \mathbf{V}_m = \mathbf{A}_m\mathbf{tm} + \mathbf{B}_m\mathbf{X} - \mathbf{l}_m & \mathbf{P}_m \\ \mathbf{V}_l = \mathbf{A}_l\mathbf{tl} + \mathbf{B}_l\mathbf{X} - \mathbf{l}_l & \mathbf{P}_l \\ \mathbf{V}_{mpos} = \mathbf{A}_{mpos}\mathbf{tm} - \mathbf{l}_{mpos} & \mathbf{P}_{mpos} \\ \mathbf{V}_{lpos} = \mathbf{A}_{lpos}\mathbf{tl} - \mathbf{l}_{lpos} & \mathbf{P}_{lpos} \\ \mathbf{V}_G = \mathbf{E}_G\mathbf{X}_G - \mathbf{l}_G & \mathbf{P}_G \end{cases} \tag{6}$$

where the last equation is the weighted observation equation of GCPs; $\mathbf{A}_m$, $\mathbf{A}_l$, $\mathbf{A}_{mpos}$, $\mathbf{A}_{lpos}$, $\mathbf{E}_G$, $\mathbf{B}_m$, $\mathbf{B}_l$ are the corresponding design matrices; $\mathbf{V}$ ($\mathbf{V}_m$, $\mathbf{V}_l$, $\mathbf{V}_{mpos}$, $\mathbf{V}_{lpos}$, $\mathbf{V}_G$), $\mathbf{l}$ ($\mathbf{l}_m$, $\mathbf{l}_l$, $\mathbf{l}_{mpos}$, $\mathbf{l}_{lpos}$, $\mathbf{l}_G$), $\mathbf{P}$ ($\mathbf{P}_m$, $\mathbf{P}_l$, $\mathbf{P}_{mpos}$, $\mathbf{P}_{lpos}$, $\mathbf{P}_G$) are the residual and discrepancy vectors, and weight matrices, respectively; $\mathbf{tm}$ and $\mathbf{tl}$ are the unknown vectors of orientation parameters of frame (matrix) array imagery and linear array imagery, respectively; and $\mathbf{X}$ and $\mathbf{X}_G$ are the object space coordinate vectors of the tie points and GCPs, respectively.

Assuming there are N_m frame array images, N_l linear array images, N_p tie points and N_G GCPs, then the total number of unknowns to be estimated is $6\times N_m + 18\times N_l + 3\times N_p + 3\times N_G$. If the GCPs are treated as errorless, the corresponding items in equation (6) should be removed.

SOLUTIONS FOR THE LARGE-SCALE NORMAL EQUATIONS

The integration of multi-source linear array and frame array imagery into a single bundle adjustment brings not only the complementary advantages of these two kinds of

imagery, but also the pressure to cope adequately with the large number of normal equations. Therefore, it is an urgent task to find a fast computational strategy to solve the normal equations of CALFI. According to the features of the unknowns in CALFI, rearranging the order of the unknowns would result in a smaller bandwidth of the reduced normal matrix (Wolf, 1983), which leads to more efficient computation and lower storage requirements when applying the recursive partitioning technique.

There are four kinds of unknown parameters in CALFI: (i) the EO parameters **tm** of the frame array imagery; (ii) the EO parameters **tl** of the linear array imagery; (iii) object space coordinates **X** of tie points; and (iv) additional parameters $\mathbf{X}_{se}$ such as systematic errors in the POS observations. In general, these four unknowns have the quantitative relationship $N_P > N_{tm} > N_{tl} > N_{se}$, where: N_P is the number of unknown object space coordinates in vector **X**; N_{tm} and N_{tl} are the number of unknown EO parameters in the frame and linear array images, respectively, in **tm** and **tl**; and N_{se} is the number of unknown additional parameters in $\mathbf{X}_{se}$.

The unknown parameters of the object space coordinates can be removed by the reduction of the normal equations. However, the reduced normal equations with the remaining unknowns (**tm**, **tl**, $\mathbf{X}_{se}$) are still too large to be directly and efficiently inverted for large block datasets. Therefore, it is necessary to use a recursive partitioning algorithm to solve the reduced normal equations. However, the sparse block-diagonal structure of the reduced normal equation matrix may be damaged if the EO parameters of frame array imagery and linear array imagery are arranged together. However, the EO parameters of one linear array image usually have connections with those of several frame array images, related by their corresponding points. Due to these connections, the off-diagonal elements in the reduced normal equation matrix that corresponds to the EO parameters of the linear array image and the connected frame array images would be non-zero. This situation causes a substantially large bandwidth of the reduced normal equation matrix. Taking the simulated sensors in the following section as an example, suppose there is a photographic area of 268 km $\times$ 225 km that covers 26 strips of linear array imagery and 50 strips of frame array imagery with 200 images in each strip. More than 14 GB of memory is required to store the reduced normal equations, which means that the normal equations are impossible to process on standard personal computers.

Therefore, the positions of the equations in the unknowns (**tm**, **tl**, $\mathbf{X}_{se}$) should be re-arranged to reduce the size of the normal matrix by firstly eliminating some unknowns and then computing them in another part of the program. Considering the fact that the number of EO parameters associated with the linear array imagery is far fewer than with the frame array imagery, it is feasible to move them into the group of additional parameters, which is located on the border of the reduced normal matrix as a banded-border structure. By this means, the sub-matrix of the EO parameters of the frame array images still maintains the sparse block-diagonal structure. Accordingly, the combination of the EO parameters of the linear array imagery and the original additional parameters as "new" additional parameters ensures the reduced normal equation matrix maintains a small bandwidth, which makes it possible to conserve memory and take advantage of the recursive partitioning technique. In this example, only about 0·8 GB of memory is needed, which means it is reasonable to solve the normal equations on standard personal computers.

Given that the orientation image model is the orientation model for the linear array imagery, the number of EO parameters of the linear array imagery is still limited, since only the orientation images have EO parameters. As a result, the quantitative relationship between the four types of unknowns would not be changed, and, in return, the presented method is still suitable for the computation of large numbers of normal equations in CALFI.

TABLE I. Parameters of the simulated frame array and linear array sensors.

Sensor	*Focal length (mm)*	*Pixel size (μm)*	*Image format (pixels)*	*Forward/ backward angle (°)*	*Flying/orbital height (m)*	*Forward overlap (%)*	*Lateral overlap (%)*	*Ground sampling distance (m)*
Frame	120	12·0	7680 × 13 824	None	6195	65	35	0·50
Linear	13 300	8·0	35 000	±22	684 000	100	40	0·41

EXPERIMENTS AND ANALYSIS

The proposed model of CALFI requires the conjugate points and POS observations of both the linear array and frame array images. However, except for SPOT 5 (which has a 5 m by 10 m ground resolution and provides a rigorous model with original orbit and attitude observations), other high-resolution satellites provide rational polynomial coefficients (RPCs) only. The ground resolution of the CCD sensors on the Chinese TH-1 satellite is also 5 m. These relatively low-resolution satellite images cannot fully take advantage of a combined bundle adjustment with aerial imagery that has a ground resolution of better than 0·5 m. Furthermore, due to financial considerations the authors did not have access to actual high-resolution datasets to perform experiments. Thus in order to verify the feasibility of CALFI, a simulated dataset was generated for the combined block adjustment experiments, which were performed to compare and analyse the precision and observational structure performance among the three modes BAFI (frame arrays only), BALI (linear arrays only) and CALFI (combined arrays).

Introduction of the Simulated Dataset

The CALFI model requires at least one type of linear array imagery and one type of frame array imagery. Therefore, the simulated experiment was carried out by a combination of airborne frame array imagery and spaceborne linear array imagery. The airborne frame CCD sensor was based on a DMC camera, while the spaceborne linear scanner was based on the parameters of the sensors in the two satellites GeoEye-1 and ZY-3. Table I shows the simulated parameters of the frame array and linear array sensors. This data combination strategy can not only guarantee the observational requirements for both linear and frame array imagery, but also can evaluate the bundle adjustment performance when using a combination of aerial and space images.

Actual digital elevation model (DEM) data of the 50 km × 50 km ground coverage area was used to generate the simulated datasets for the experiments. The following procedure for generating the simulated observations was utilised. The flights and corresponding GNSS/IMU measurements of the frame and linear array sensors were generated first. Then, discrete 3D points were sampled as tie points from the actual DEM of the test area, and the image points of both the linear array and frame array images were generated by backward projection. Finally, Gaussian noise was introduced into the observations as follows: 2·0 μm standard deviation for the image points; 0·2 m and 2·0″ standard deviations for the GNSS and IMU measurements, respectively; and 0·1 m standard deviation for the GCPs.

Experiments and Analysis of Accuracy

Two simulation experiments will be discussed in this section: (i) an experiment on the change of precision with different strip lengths; and (ii) an experiment on the precision with a fixed block size. The first experiment provides a general comparison of precision between

the three types of adjustment, while the second analyses the precision dependent upon the distribution of tie points. In the two experiments, the weight of each observation was determined according to its nominal accuracy. Contrary to the strategy adopted by Wu et al. (2011) which changed the weights of the EO parameters by a fixed step, the weight of each observation in this paper was determined by its ground uncertainty, which was calculated by the intentionally added Gaussian noise. For example, the ground resolution of the frame aerial imagery and the linear array satellite imagery was 0·5 and 0·4 m, respectively, so the image coordinate uncertainty was around 0·08 and 0·10 m, respectively, since the Gaussian noise of the image point was 2·0 μm. The ground uncertainty of IMU observations' roll and pitch was determined by multiplying the flying height by their 2·0″ nominal standard deviation, while the ground uncertainty of yaw observations was determined by multiplying the ground coverage or swath width by the 2·0″ nominal standard deviation. The weights of image points of the aerial images were set to be 1·0, which corresponds to a unit weight of 0·08 m in the object space. The weights of all the other observations were calculated as the squared ratio of 0·08 m against their corresponding ground uncertainties; for example, the weights of the GNSS observations were $(0{\cdot}08/0{\cdot}2)^2 = 0{\cdot}16$.

Accuracy Indicator in the Experiment. The precision of the tie points can be determined by the diagonal element of the variance and covariance matrix, or by the differences between the computed coordinates and the field-measured coordinates. In this experiment, the true values for the object space coordinates of the tie points are known. As a result, the actual accuracy of block adjustment can be obtained by calculating the differences between the adjusted coordinates and the true coordinates from the simulated data. The horizontal and vertical accuracies are estimated by the root mean values of the squared differences between the computed and true coordinates of tie points.

Accuracy of the Three Adjustment Modes with Different Strip Lengths. The objective of this experiment was to investigate the change in precision of the three types of adjustment (BAFI, BALI and CALFI) with different strip lengths, varying from 4 to 29 images per strip. Four GCPs located at the four corners of the block, which comprised three strips of frame array images and two strips of linear array images, were used for this experiment.

As illustrated in Fig. 2, where the four GCPs are located at each corner of the block, the horizontal and vertical accuracies of the POS-supported bundle adjustment with frame array imagery (BAFI) are very stable (about 0·2 and 0·25 m, respectively). The horizontal accuracy of the POS-supported bundle adjustment with linear array images (BALI) is slightly better than the frame array images. However, the vertical accuracy of the linear array imagery was less stable and exhibited increasing variations with strip length, decreasing the precision from 0·25 to 0·4 m. One reason for this decrease was that the added random error on the linear array image point was about 1/4 pixel, which was larger than the 1/6 pixel of the frame array image point. Furthermore, the systematic accumulation of random errors also contributed to the decrease in vertical accuracy. Taking advantage of the combination of linear array and frame array images, and assisted by the POS observations, the CALFI model provides both the best horizontal and vertical accuracies. The improvement in horizontal accuracy by using CALFI was between 29 and 53% over BAFI, and by 23 to 45% over BALI; the equivalent vertical accuracies improved by 23 to 43% and 42 to 60%, respectively, by using CALFI.

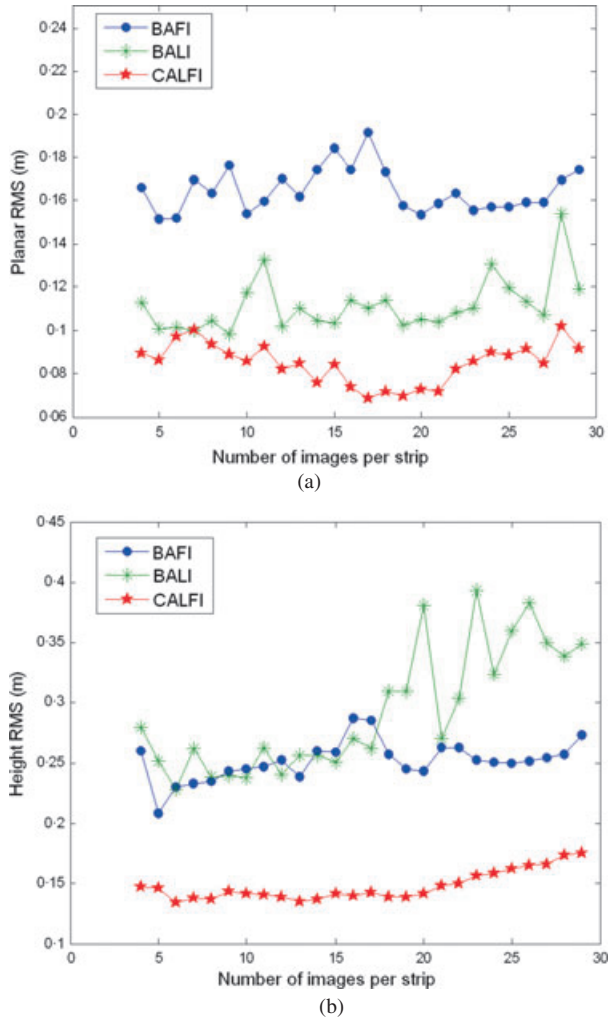

FIG. 2. Horizontal and vertical precision of the three modes with different strip length.

Accuracy of the Three Adjustment Modes with Fixed Size Blocks. This experiment aimed to compare and analyse the accuracy distribution of the tie points of the three adjustment modes in a small block containing: (i) three strips of frame array imagery with seven images in each strip; and (ii) two strips of linear array images. There were 232 regularly distributed ground points within the test area. As shown in Figs. 3 and 4, every cross (×) represents a tie point which has three precision values from BAFI, BALI and CALFI, marked by lines with different hues and lengths. The length of a certain line is proportional to the absolute difference between the adjusted coordinate and the true coordinate (the longer the line, the lower the accuracy).

It can be observed in Figs. 3 and 4 that most of the tie points of CALFI have both the highest horizontal and vertical accuracy. This result is in agreement with the experiment in

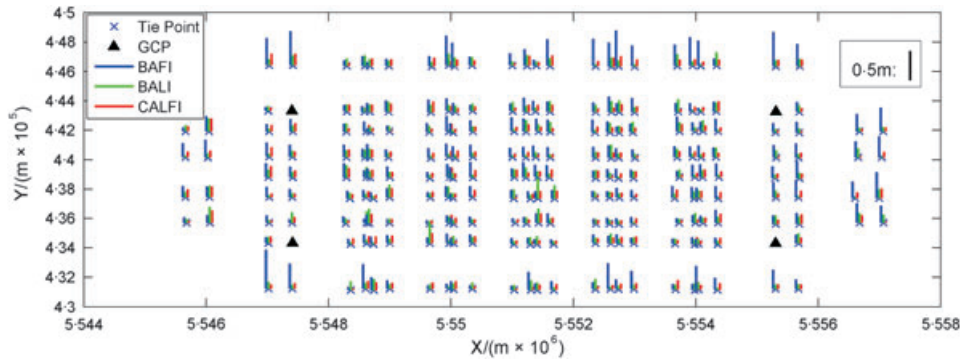

FIG. 3. Horizontal precision distribution of tie points with the three different adjustment modes.

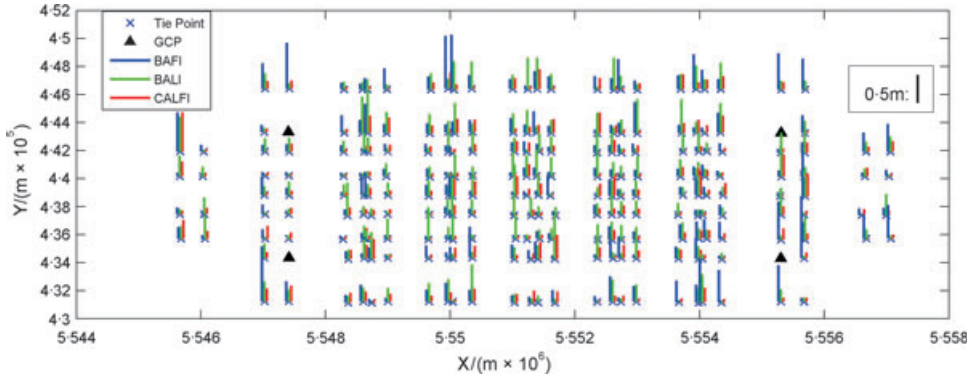

FIG. 4. Vertical precision distribution of tie points with the three different adjustment modes.

the above section. The accuracy of the tie points of BAFI or BALI on the periphery of the test area was worse when compared to the internal area, which accords with the results of Ackermann (1975). The accuracy of the tie points of CALFI was only slightly influenced by the location of the tie points within the block.

The above two experimental results show that CALFI was more accurate, both horizontally and vertically, than either BAFI and BALI. The improvement in accuracy is a consequence of having more rays per point and a better observational structure by combining different spaceborne and airborne sensors; the combined data from two separate acquisitions has more constraints than either of the two individual acquisitions.

Analysis of Observational Structure

Measure of Observational Structure. In addition to the accuracy of the adjustment, the ill-conditioned problem is another important concern in the field of least squares adjustment. Observational structure is used to denote a special form, or condition, of observational weakness that causes the estimated parameters to be very sensitive to small perturbations in the observation data (Belsley, 1991). Over many decades, several procedures or measures have been proposed to diagnose the ill-conditioned problem, or multicollinearity, such as

the correlation matrix, the eigenvalues and eigenvectors of the observation matrix, and the Farrar and Glauber technique (Farral et al., 1967).

As discussed previously, the integration of linear array and frame array imagery from different sensors, with different flying/orbital heights and different viewing angles, is theoretically capable of providing a more comprehensive, and thus better, observational structure. In order to investigate and confirm this idea, the above experimental data with the fixed size block is again used to compare the observational structure, or multicollinearity, of the three adjustment modes. Accordingly, two measures for diagnosing multicollinearity, as presented by Belsley (1991), were employed.

(1) *Determinant of the normal equation matrix* $\mathbf{N} = \mathbf{A}^{\mathrm{T}}\mathbf{A}$

A design matrix $\underset{m\times n}{\mathbf{A}} = [a_1 \quad a_2 \quad \cdots \quad a_n]$ can be assumed to be a super polyhedron with each side a_i ($i = 1,2,\ldots, n$) in an m-dimensional space. The volume of the super polyhedron is an important geometric indicator for the observational structure of the design matrix $\mathbf{A}$; according to Belsley (1991) the greater the volume, the better conditioned the observations. It is known that the volume of the polyhedron is equal to the square root of the determinant of the Gram matrix of $\mathbf{A}$, $G(\mathbf{A})$:

$$\mathrm{Vol}(\mathbf{A}) = \sqrt{\det(G(\mathbf{A}))} = \sqrt{\det(\mathbf{A}^{\mathrm{T}}\mathbf{A})} = \sqrt{\det(\mathbf{N})}. \tag{7}$$

Therefore, the determinant $\det(\mathbf{N})$ is applied as the first indicator to measure the observational structure.

(2) *Condition number of the normal equation matrix* $\mathbf{N} = \mathbf{A}^{\mathrm{T}}\mathbf{A}$

The condition number is a classic index for collinearity diagnosis. It is also employed in this experiment as the indicator of observation structure. According to the definition of the condition number (Belsley, 1991):

$$\kappa(\mathbf{N}) = \frac{\lambda_{\max}(\mathbf{N})}{\lambda_{\min}(\mathbf{N})} \geq 1 \tag{8}$$

where $\lambda_{\max}(\mathbf{N})$, $\lambda_{\min}(\mathbf{N})$ are the maximum and minimum eigenvalues of $\mathbf{N}$, respectively, and $\kappa(\mathbf{N})$ is the condition number which represents the ratio of the minimum eigenvalue to the maximum one. The presence of small eigenvalues of $\mathbf{N}$ indicates the presence of ill-conditioning (multicollinearity) among the columns of $\mathbf{A}$. An eigenvalue close to zero means there is an approximate linear dependency among the columns of $\mathbf{A}$. The condition number, therefore, can be used to measure the sensitivity of the least squares adjustment to the strength of the design matrix and the observations. In other words, the closer the condition number is to one, the better the observational structure of the adjustment system.

Observational Structure of the Three Adjustment Modes with Fixed Size Block. As already described, three strips of frame array imagery with seven images in each strip, and two strips of linear array imagery, were used for the experiment, resulting in a total of 232 tie points in the block.

In order to compare the observational structures of the three adjustment modes, the determinant and condition number measures $\det(\mathbf{N})$ and $\kappa(\mathbf{N})$ were employed. Both of these

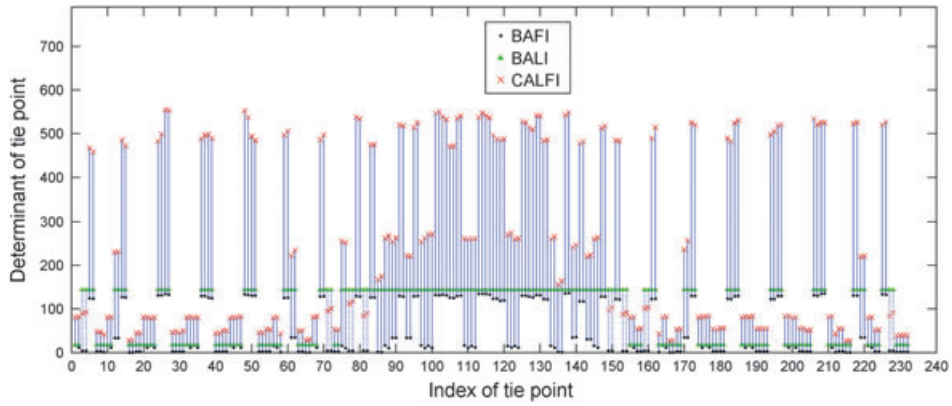

FIG. 5. Determinant of normalised design matrix of tie point with three adjustment modes.

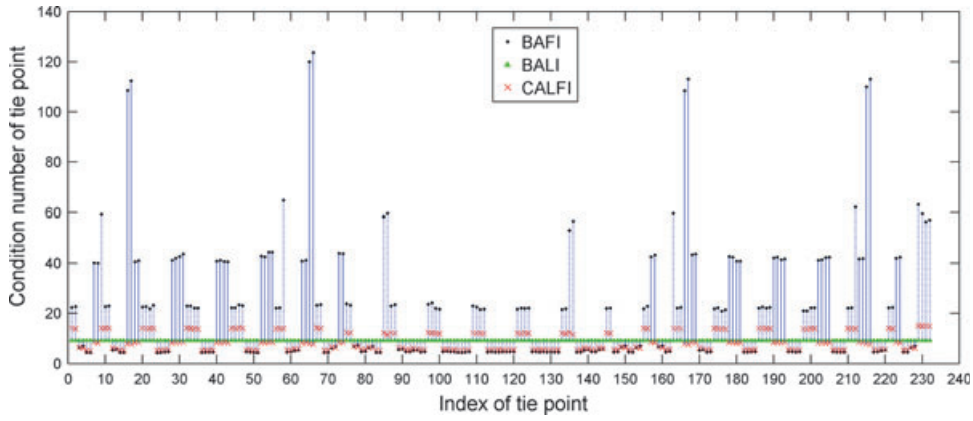

FIG. 6. Condition number of design matrix of tie point with three adjustment modes.

were derived from the design matrix **A** in the block adjustment. However, it was neither convenient nor practical to use all the entries of the design matrix for three reasons. Firstly, the size of matrix **A** was too enormous to efficiently compute the determinant or the condition number. Secondly, matrix **A** included information about the conditioning of both the EO parameters and the tie points, whereas the elements of the EO parameters in the three adjustment modes were different from each other and not comparable. Thirdly, the precision and robustness of the tie points, rather than the EO parameters, were the real focus of concern. Based on these considerations, the computation for the entire design matrix **A** was converted to compute the sub-design matrix $\underset{n\times 3}{\mathbf{A}}(P_i)$ of every tie point, where P_i indicates the *i*th tie point. Consequently, the observational structure of the three adjustment modes was measured and compared by the determinant and condition number of each tie point's sub-design matrix $\underset{n\times 3}{\mathbf{A}}(P_i)$. The determinant and condition number indicators of each point of the three adjustment modes are shown in Figs. 5 and 6, where dots represent BAFI, triangles represent BALI and crosses represent CALFI. There are 216 solid vertical lines in Fig. 5 (93% of the total) representing the improvement due to CALFI. The 16 pecked

TABLE II. Average statistics of the conditioning of all tie points.

Statistics	$det(\mathbf{N})$	$cond(\mathbf{A})$
BAFI	51·213	22·438
BALI	91·895	9·187
CALFI	250·023	8·569

vertical lines represent the far fewer points where the linear array adjustment alone (BALI) produced better results than the combined CALFI adjustment. This means most of the tie points have the best observation structure under CALFI when the determinant is the indicator.

When calculating the determinant of the design matrix $\det(\underset{n\times 3}{\mathbf{A}}(\mathrm{P}_i))$, $\underset{n\times 3}{\mathbf{A}}(\mathrm{P}_i)$ was normalised to $[-1, 1]$ for better analysis because the original elements of the design matrix were very small. Table II shows the average statistics of the conditioning measures of all of the tie points of the three adjustment modes.

Figs. 5 and 6 indicate that the conditioning measures of the different tie points of BALI showed little change owing to the stable observation structure of the three linear array sensors. The conditioning of the tie points of BAFI in the middle part of both figures was better than that of the left and right parts because these tie points were in the second strip and also were photographed in the first and the third strips, thus improving the observation structure. The distinctive patterns evident in Figs. 5 and 6 are dependent on the tie point index, in other words the numbering of the tie points. As shown in Figs. 3 and 4, there are nine rows of tie points in the block. The numbering (index) of tie points (abscissae in Figs. 5 and 6) increases from left to right within a certain row of tie points, and then row by row from top to bottom. For example, the first point is located at the top-left corner of Fig. 3 and the last point is located at the bottom-right corner. The patterns observed in Figs. 5 and 6 are mainly related to the position of a certain point within the block. For example, all the BALI results appear to have determinants of either about 130 or 20 in Fig. 5. In general, the result of a point located towards the centre of the block, which means it has more conjugate image points, is better than the result of a point located at the margins of the block that has fewer conjugate points. As can be seen from Fig. 6, there are eight frame array points with a condition number exceeding 100. These points are located at the very periphery of the block and beyond the area linking the four GCPs. Fig. 6 also shows that the overall condition number of the tie points of CALFI was the best. From an overall perspective, by referring to Table II, the model of CALFI exhibited the best observation structure with regard to both $\det(\mathbf{N})$ and $\kappa(\mathbf{N})$. It should be noted that a different configuration of images, strips and GCPs would produce different patterns, but these are likely to reflect the above results.

Based on the above two simulated experiments, it can be seen that, due to the complementary advantages of the combination of linear array and frame array imagery, CALFI produced better adjustment performance in terms of the accuracy and observation structure compared to both BAFI and BALI.

CONCLUSIONS

This paper has established the mathematical model of CALFI, which was based on the conventional models of BALI and BAFI, including the use of quadratic polynomials as the orientation model of linear array imagery. Considering the large number of the (four types of) unknown parameters in CALFI, a revised recursive partitioning algorithm to solve the

large-scale normal equation was proposed. To speed up the computation efficiency and to make it practicable, the EO parameters of the linear array imagery were treated as additional parameters and were moved to the border of the reduced normal equation. Finally, in the simulated experiments, the feasibility and superiority of CALFI were verified by comparing the accuracy and observation structure performance of the three adjustment modes.

A drawback of the results presented is that the authors did not have access to actual high-resolution datasets to perform the experiments. Future research will focus on utilising real datasets to test and improve the CALFI model. Automatic determination of the weights of the different observations also needs to be investigated. Furthermore, an orientation image model should be used to deal with long strip linear array imagery.

Acknowledgement

This work was supported in part by the National Basic Research Programme of China (Project No. 2012CB719904), the National Natural Science Foundation of China (Project Nos. 41071233 and 41171292) and the National Key Technology Research and Development Programme (Project No. 2011BAH12B05 and 2013AA12A401). Heartfelt thanks are also given for the comments and contributions of reviewers and members of the editorial team.

References

Ackermann, F., 1975. Results of recent test in aerial triangulation. *Photogrammetric Engineering & Remote Sensing*, 41(1): 91–99.

Ackermann, F., 1995. Sensor and data integration – the new challenge. *Proceedings of ISPRS Workshop on Integrated Sensor Orientation*, Barcelona, Spain. 2–10.

Belsley, D. A., 1991. *Conditioning Diagnostics: Collinearity and Weak Data in Regression*. Wiley, Chichester. 396 pages.

Cariou, C. and Chehdi, K., 2008. Automatic georeferencing of airborne pushbroom scanner images with missing ancillary data using mutual information. *IEEE Transactions on Geoscience and Remote Sensing*, 46(5): 1290–1300.

Farrar, D. E. and Glauber, R. R., 1967. Multicollinearity in regression analysis: the problem revisited. *The Review of Economics and Statistics*, 49(1): 92–107.

Greening, W. J. T., Schickler, W. and Thorpe, A. J., 2000. The proper use of directly observed orientation data: aerial triangulation is not obsolete. *Proceedings of ASPRS Annual Conference*, Washington, DC, USA. 12 pages (on CD-ROM).

Gruen, A. and Zhang, L., 2003. Sensor modeling for aerial triangulation with Three-Line-Scanner (TLS) imagery. *Photogrammetrie, Fernerkundung, Geoinformation*, 2/2003: 85–98.

Gugan, D. J., 1987. Practical aspects of topographic mapping from SPOT imagery. *Photogrammetric Record*, 12(69): 349–355.

Habib, A. and Beshah, B., 1998. Multi sensor aerial triangulation. *International Archives of Photogrammetry and Remote Sensing*, 32(3): 37–41.

Kocaman, S. and Gruen, A., 2008. Orientation and self-calibration of ALOS PRISM imagery. *Photogrammetric Record*, 23(123): 323–340.

Lee, C., Theiss, H. J., Bethel, J. S. and Mikhail, E. M., 2000. Rigorous mathematical modeling of airborne pushbroom imaging systems. *Photogrammetric Engineering & Remote Sensing*, 66(4): 385–392.

Li, D., Shan, J. and Gong, J. Y. (Eds.), 2009. *Geospatial Technology for Earth Observation*. Springer, New York, USA. 556 pages.

Li, R. X., Deshpande, S., Niu, X. T., Zhou, F., Di, K. C. and Wu, B., 2008. Geometric integration of aerial and high-resolution satellite imagery and application in shoreline mapping. *Marine Geodesy*, 31(3): 143–159.

Orun, A. B. and Natarajan, K., 1994. A modified bundle adjustment software for SPOT imagery and photography: tradeoff. *Photogrammetric Engineering & Remote Sensing*, 60(12): 1431–1437.

Poli, D., 2004. Orientation of satellite and airborne imagery from multi-line pushbroom sensors with a rigorous sensor model. *International Archives of Photogrammetry, Remote Sensing and Spatial Information Sciences*, 35(B1): 130–135.

SCHENK, T., 2003. Progress in automatic aerial triangulation. *Photogrammetric Week*, Stuttgart, Germany. 129–140.
SHIN, S. W., HABIB, A. F., GHANMA, M., KIM, C. and KIM, E.-M., 2007. Algorithms for multi-sensor and multi-primitive photogrammetric triangulation. *ETRI Journal*, 29(4): 411–420.
WANG, R. X., HU, X., YANG, J. F. and WANG, X. Y., 2004. Proposal to use LMCCD camera for satellite photogrammetry. *Acta Geodaetica et Cartographica Sinica*, 33(2): 117–120.
WOLF, P. R., 1983. *Elements of Photogrammetry*. Second edition. McGraw-Hill, New York, USA. 628 pages.
WU, B., GUO, J., ZHANG, Y. S., KING, B. A., LI, Z. L. and CHEN, Y. Q., 2011. Integration of Chang'E-1 imagery and laser altimeter data for precision lunar topographic modeling. *IEEE Transactions on Geoscience and Remote Sensing*, 49(12): 4889–4903.
ZHANG, Y. J., ZHANG, Z. X., ZHANG, J. Q. and WU, J., 2005. 3D building modelling with digital map, lidar data and video image sequences. *Photogrammetric Record*, 20(111): 285–302.
ZHANG, Y. J., XIONG, J. X. and HAO, L. J., 2011. Photogrammetric processing of low-altitude images acquired by unpiloted aerial vehicles. *Photogrammetric Record*, 26(134): 190–211.

Résumé

L'intégration de données multi-capteurs d'observation de la Terre est devenue l'un des développements majeurs de photogrammétrie. Un ajustement combiné d'images acquises par des capteurs à barrette et à matrice de détecteurs (dit CALFI) est établi dans cet article. Le modèle mathématique de CALFI s'appuie sur une classique compensation par faisceaux mono-capteur. Une technique de partition récursive adaptée est utilisée pour résoudre la grande matrice normale de CALFI. Les paramètres d'orientation de l'image à barrette sont disposés sur le bord de la matrice normale réduite pour économiser de la mémoire ainsi que du temps de calcul. Les résultats expérimentaux montrent que le modèle CALFI améliore la précision ainsi que l'indice de conditionnement par rapport au modèle conventionnel de compensation par faisceaux, pour l'image à barrette comme pour l'image à matrice, prises séparément, en raison d'une plus grande redondance.

Zusammenfassung

Die Integration von Multi-Sensor Daten ist eine der wichtigsten Entwicklungen in der heutigen Photogrammetrie. Dieser Beitrag stellt eine kombinierte Ausgleichung von Zeilen- und Flächenkameras (CALFI) vor. Das mathematische Modell von CALFI stützt sich auf die konventionelle Bündelausgleichung mit einer Kamerageometrie. Zur Lösung der großen Normalgleichungsmatrix von CALFI wird eine überarbeitete, rekursive Partitionierungstechnik verwendet. Dabei werden die Orientierungsparameter der Zeilenbilder am Rand der reduzierten Normalgleichungsmatrix angeordnet, um sowohl Speicherplatz, als auch Rechenzeit zu sparen. Experimentelle Ergebnisse zeigen, dass die Genauigkeit und die Konditionszahl des CALFI Modells wegen der höheren Redundanz besser sind, als bei einer getrennten klassischen Bündelausgleichung der Zeilen- und Flächenbilder.

Resumen

Uno de los más importantes desarrollos en fotogrametrŏa es la integración de múltiples sensores. En este trabajo establecemos un ajuste combinado de imágenes de sensores de lőnea y de cuadro (CALFI). El modelo matemático del CALFI se basa en las ecuaciones convencionales del ajuste de haces con imágenes de un sólo sensor. Para resolver la gran matriz normal se hacen particiones de forma recursiva y revisada; los parámetros de orientación del sensor de lőnea se ordenan al extremo de la matriz normal reducida para ahorrar memoria y tiempo de cálculo. Los resultados experimentales muestran que tanto la precisión cómo el número de condición del modelo CALFI son superiores al modelo de ajuste de haces convencional ya sea con sensores de lőnea o de cuadro separadamente debido a su mayor redundancia.